Springer

KSME

Journal of Mechanical Science and Technology 25 (9) (2011) 2237~2246
www.springerlink.com/content/1738-494x
DOI 10.1007/s12206-011-0706-3

A general structural design methodology for multi-hole orifices and its experimental application †

Tianyi Zhao*, Jili Zhang and Liangdong Ma

School of Civil Engineering, Faculty of Infrastructure Engineering, Dalian University of Technology, Dalian, China

(Manuscript Received August 20, 2010; Revised March 7, 2011; Accepted May 27, 2011)

Abstract

Compared to single-hole orifices (SOs), multi-hole orifices (MOs) have smaller orifice sizes and various patterns of orifice distribution. The geometric description of MOs is more complex, increasing the difficulty of MO structural design. Therefore, it is worthwhile to investigate the key factors affecting MO throttle or flow control characteristics and to develop a general MO design method. This work presents a practical geometric design methodology for MOs and applies this procedure in throttle experiments. To describe the MO geometry in detail, the methodology first introduces a comprehensive set of geometric architectures involving orifice arrangement criteria and geometric parameters such as the total orifice number, n; the orifice distribution density, Dd; and the equivalent diameter ratio, EDR. Then, a series of throttle tests in water flow are conducted to investigate the effect of various geometric features on the pressure loss characteristics of MOs. Finally, a simple model to calculate the pressure loss coefficient of MOs is presented.

Keywords: Multi-hole orifice; Pressure loss coefficient; Structural design methodology; Throttle test

1. Introduction

Orifice plates are widely used as throttle fittings in refrigeration and heat pump systems. Fig. 1 shows an electric expansion valve that uses circular orifices as throttle devices. The orifices are installed at the bottom of the expansion valve. Liquid refrigerant flows through the orifices and flashes to gas because of the pressure drop created by the orifices. Refrigerant mass flow is regulated by the motor-driven screw stem.

Fig. 2 shows an integrated evaporator condenser in which the condenser and evaporator are separated by the thermal baffle and the orifice plate that throttle the refrigerant drawn from the condenser into the evaporator. The orifice can also regulate refrigerant mass flow when the difference between the evaporate and condensate pressures changes.

Fig. 3 describes the configuration of a two-stage MO fitting applied in some refrigeration systems.

As Fig. 3(a) shows, the flow of liquid refrigerant through the primary orifice occurs without a phase change because the refrigerant generally has a higher entry pressure in the full load condition. After the primary throttle process, the refrigerant passes through the secondary MO and flashes to gas.

In Fig. 3(b), the phase change of the liquid refrigerant occurs through the primary MO because the refrigerant experiences a pressure decrease in the partial load condition. As a consequence, the gas-liquid refrigerant flows across the secondary MO, and the gas lock phenomenon occurs at the micro-size perforated holes, which decreases the refrigerant mass flow entering the evaporator and induces a flow adaptation effect on the throttle fitting.

The removable design shown in Fig. 3(c) allows the pres-

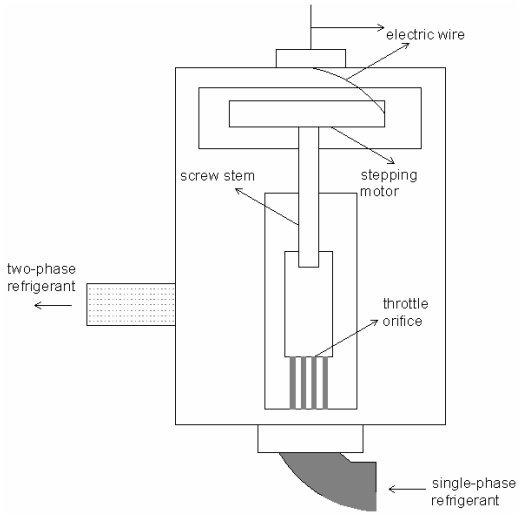

Fig. 1. Typical electric expansion valve.

† This paper was recommended for publication in revised form by Associate Editor Simon Song

* Corresponding author. Tel.: +86 411 84707753, Fax.: +86 411 84707753
E-mail address: sebastian.zhao@gmail.com

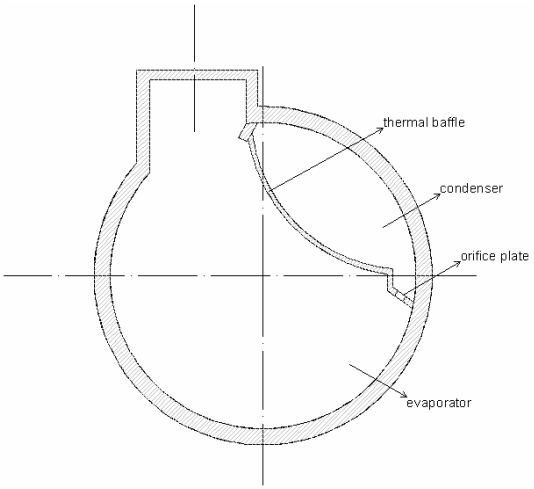

Fig. 2. Integrated evaporator condenser.

sure loss coefficient of the integrated throttle fitting to be adjusted by changing the position of the movable MO. This is another novel way to realize adaptive flow regulation.

According to the above illustration, MOs appear to have various potential applications because of their convenience and low cost, but more work is needed to realize these applications. The uncertain orifice arrangement and complex geometric features of MOs complicate their structural description and design, greatly restricting the application of MOs. To solve this problem, a general MO structural design methodology needs to be investigated, and a simple MO pressure loss model needs to be further studied.

With particular reference to orifice geometry and pressure loss characteristics, in his early study, Anderson [1] related the dependence of the primary frequency on differential pressure to the orifice geometry with a circular-orifice number. The acoustic effects of cavitation were discussed by testing a circular-centered single-hole orifice and a multi-hole orifice by P. Testud et al. [2]. The pressure loss coefficients of square-edged orifices and perforated plates were determined by Guohui Gan et al. [3]. Some researchers have studied two-phase flows: M. Fossa et al. [4] investigated two-phase flow pressure drop and void fraction profiles with respect to the effect of the area contraction ratios and orifice thicknesses. G. Kojasoy conducted a similar study on two-phase pressure drops in multiple thick and thin orifice plates [5]. Saadawi et al. conducted experimental investigations of two-phase flows across orifices in large diameter pipes [6].

As shown by the above literature review, few studies have investigated the structural design issue of orifices, especially MOs. Even in the few studies involving MOs, a comprehensive set of geometric orifice parameters and their influences on the MO pressure loss coefficient were not sufficiently addressed.

This paper presents a novel and general methodology for MO geometric design, and this method was applied in a series of throttle tests under single-phase conditions. A simple pressure loss coefficient model of test MOs is provided based on the design methodology and test results.

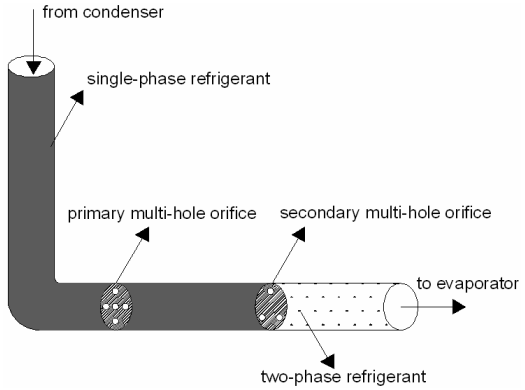

(a) Full load condition

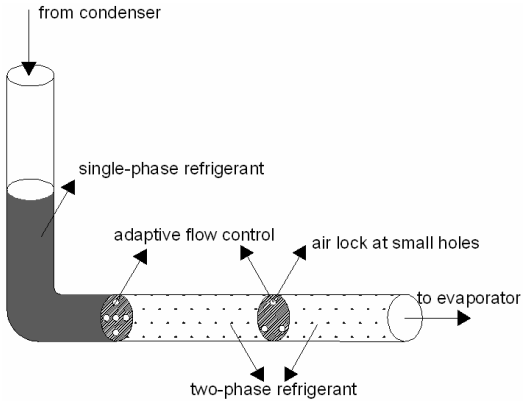

(b) Partial load condition

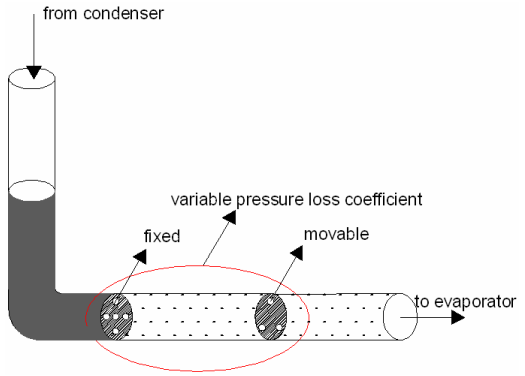

(c) Removable design

Fig. 3. Two-stage multi-hole orifice throttle device.

2. Methodology conception

MO geometry and refrigerant properties are both known to affect the pressure drop across MOs under two-phase conditions. Generally, a large body of test data is needed to determine the correlation between these two characteristics and the MO pressure loss. For convenience, this paper emphasizes the MO geometry effect and leaves the influence of the refrigerant

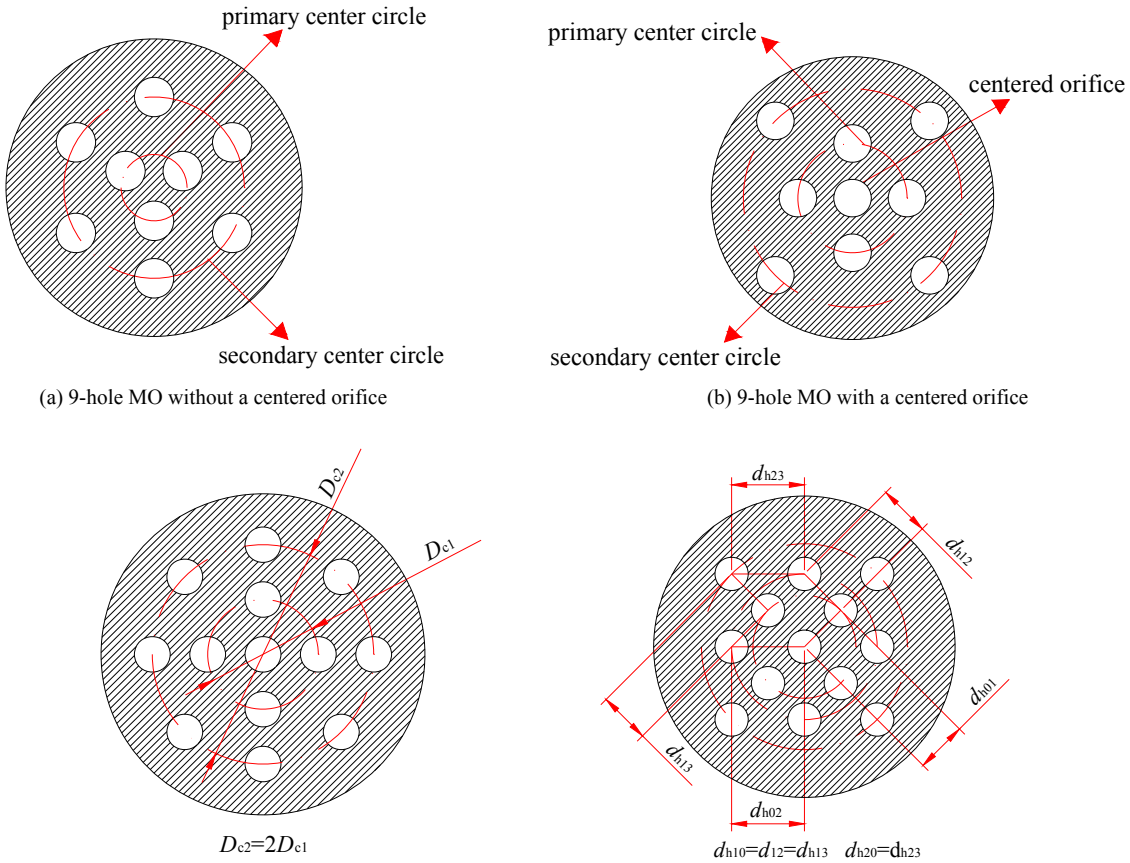

(a) 9-hole MO without a centered orifice

(b) 9-hole MO with a centered orifice

(c) 13-hole MO with a circular arrangement

(d) 13-hole MO with a rectangular arrangement

Fig. 4. Description of the orifice arrangement.

flashing process on MO throttle capability for consideration by future studies. Therefore, the throttle tests in this work were conducted under water flow.

In present work, the presented methodology mainly consists of the definition of the MO geometric architecture and two-stage throttle experiments. The primary experimental stage investigated how the different geometric features mentioned in MO geometric architecture affect the MO pressure loss coefficient. The secondary experimental stage constructed a model of the MO pressure loss coefficient based on the dominant geometric parameter extraction study conducted in the primary experimental stage.

3. MO geometric architecture

3.1 Orifice arrangement criteria

The random number and arrangement of orifices leads to the complexity of MO geometry. To avoid this complexity, the following criteria were defined for all MOs discussed in the present work.

(1) All holes in each MO have a uniform size and are manufactured using the same technique. The orifice plate thickness was 2 mm. Detailed craft specifications were according to ISO5167-1 [9].

(2) Each orifice center was located in a set of concentric circles defined as center circles, as shown in Fig. 4(a), (b).

(3) Orifice arrangement should be as symmetrical as possible, and the spacing among most orifice centers should be equal.

(4) The total orifice number ranged from 3 to 13, and the maximum number of center circles was 3.

The various patterns of orifice arrangement can be further categorized as follows:

(1) MOs were prepared with or without a centered orifice, as shown for typical 9-hole MOs in Fig. 4(a) and (b), respectively.

(2) Two different center circle arrangements were considered in the present work. The first mode is a circular arrangement, in which the center circle location was primarily fixed according to the correlation $D_{cn}=nD_{c1}$, resulting in symmetric orifices located around these center circles as shown in Fig. 4(c).

The second mode is a rectangular arrangement with four orifices at each center circle. This arrangement primarily considers the consistency of the spacing between each orifice center, resulting in fixed center circle locations as shown in Fig. 4(d).

The circular arrangement is better bedded than the rectan-

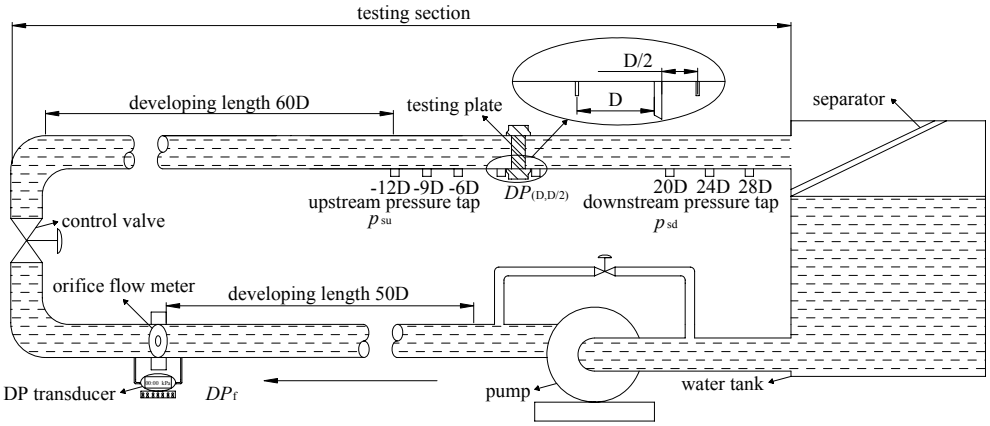

Fig. 5. Schematic of the test rig.

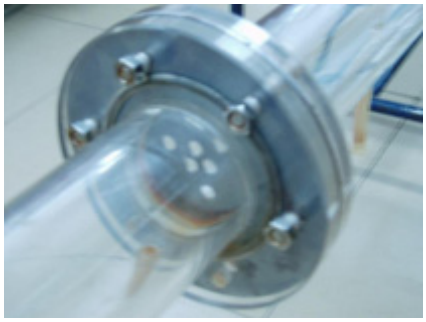

Fig. 6. A portion of the test section.

gular arrangement, and the location of the center circle is not restricted by the orifice spacing, while the rectangular arrangement has a more symmetric orifice distribution and the orifice spacing controls the location of the center circle.

3.2 Key geometric parameters

According to the above definitions, the following three geometric parameters were used to quantitatively characterize the MO geometry.

(1) The total orifice number, n.

(2) The equivalent diameter ratio, *EDR*, which represents the square root of the total open area ratio and is expressed as $n^{0.5}d/D$. *EDR* has the same geometric meaning as the diameter ratio defined for SO specified in ISO5167.

(3) The orifice distribution density D_d, which is expressed as d_{hmin}/D, where d_{hmin} represents the minimum spacing between the edges of the orifices located at adjacent center circles.

The above arrangement criteria and geometric parameters can be used to explicitly describe the MO geometry.

4. Experimental set-up

4.1 Experimental theory

This paper adopts the pressure loss coefficient to represent the local MO pressure drop characteristics. The pressure loss coefficient, ξ, is defined as

$$\xi = \frac{\Delta P_s}{P_v}. \tag{1}$$

Relative relations can be expressed as

$$\Delta P_s = p_{su} - p_{sd} \tag{2}$$

$$P_v = \frac{1}{2}\rho v^2 \tag{3}$$

$$v = \frac{4Q_v}{\pi D^2} \tag{4}$$

$$Q_v = k_f\sqrt{\frac{\Delta P_f}{\rho}}. \tag{5}$$

In Eq. (5), k_f is a transformation factor provided by the flowmeter manufacturer. Starting from Eqs. (1)-(5), ξ can be rewritten as in Eq. (6) in terms of p_{su}, p_{sd} and ΔP_f, which can be directly experimentally measured.

$$\xi = \frac{\pi^2 D^4}{8k_f^2\Delta P_f}(p_{su} - p_{sd}) \tag{6}$$

4.2 Test rig

The experimental data were obtained from the test rig shown in Fig. 5. The rig mainly consisted of a testing section, an orifice flowmeter and pressure transducers. The testing section was 6 m long. A transparent horizontal pipe with an inner diameter, D, of 50 mm was chosen to investigate the flow pattern. The test orifice plate was fixed on a test section with a flange connection (shown in Fig. 6). Dematerialized tap water was used in all experiments with a water velocity from 0.1 m/s to 1 m/s.

The test section was equipped with eight pressure taps. The static pressure differences for ξ calculations were obtained by two mean values collected by tapping at distances of 6D, 9D and 12D upstream and distances of 20D, 24D and 28D, aver-

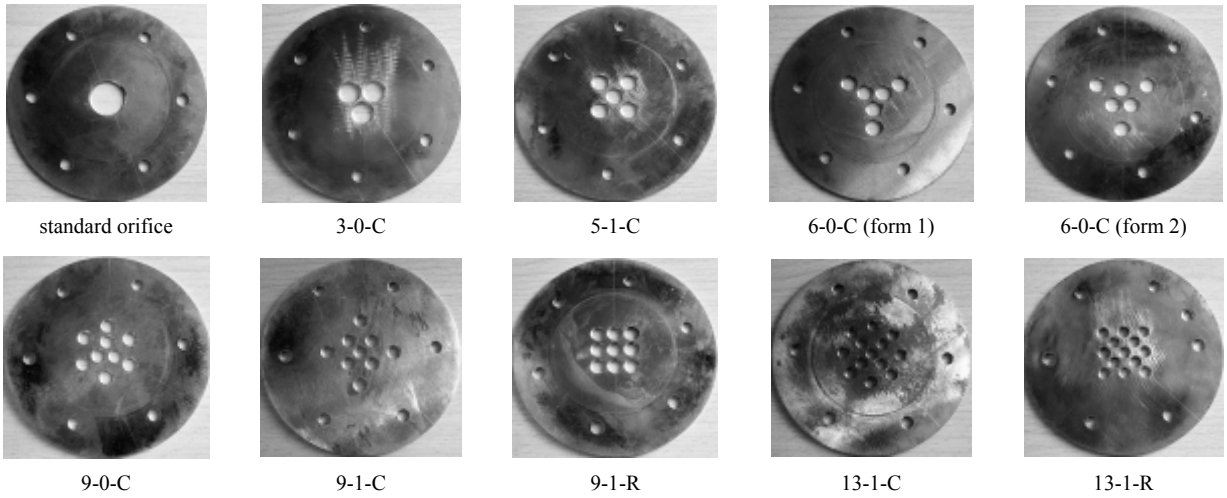

Fig. 7. Test plates employed in test 1.

aged separately. The test section was also equipped with two pressure taps located at a distance of D upstream and D/2 downstream to compare the test results with the correlations in ISO 5167. This test rig was used to obtain profiles of the pressure drop versus the mass of water flowing through the test orifice plate, providing a comprehensive characterization of the pressure loss of each test orifice.

4.3 Experimental error analysis

The relative error of the pressure loss coefficient, RE (ξ), was evaluated by Eq. (7) using the error combination law on Eq. (6) and measuring the error of the relative testing instrument.

$$\mathrm{RE}(\xi)=\sqrt{\left(\frac{\mathrm{AE}(\Delta P_{\mathrm{f}})}{\Delta P_{\mathrm{f}}}\right)^2+\left(\frac{\mathrm{AE}(p_{\mathrm{su}})}{\Delta P_{\mathrm{s}}}\right)^2+\left(\frac{\mathrm{AE}(p_{\mathrm{sd}})}{\Delta P_{\mathrm{s}}}\right)^2+16\left(\frac{\mathrm{AE}(D)}{D}\right)^2+4(\mathrm{RE}_{\mathrm{so}}(Q_{\mathrm{v}}))^2} \tag{7}$$

where REso(Q_v) refers to the relative error of Q_v associated with the flowmeter used for measurement. This term can be neglected, as can AE(D)/D; the values of these terms are small compared with the measurement error generated by the pressure transducers.

Suppose that the measurement errors of all transducers used in the test were equal. The, the errors can all be expressed as $\mathrm{AE}(\Delta P_{\mathrm{f}})=\mathrm{AE}(\Delta P_{\mathrm{su}})=\mathrm{AE}(\Delta P_{\mathrm{sd}})=\mathrm{AE}(\text{transducer})$, and Eq. (7) can be rewritten as

$$\mathrm{RE}(\xi)=\mathrm{AE}(\text{transducer})\sqrt{(\Delta P_f)^{-2}+2(\Delta P_s)^{-2}}\ . \tag{8}$$

According to Eq. (8), the transducer accuracy should satisfy the 0.1% requirement to ensure that the maximum RE(ξ) is less than 5% under the worst-case condition.

4.4 Experimental layout

ξ is known to be dominated by the geometric features of singularity in the square resistance region, including the orifice arrangement and the three geometric parameters discussed above.

Therefore, the following test can be divided into the test of the MO geometric features and the MO ξ modeling test. The primary testing stage analyzed the effect of the orifice arrangement and key geometric parameters on ξ to simplify the quantitative description of the MO geometry for modeling. The secondary testing stage proposed a ξ correlation based on the test data.

5. Testing the effects of MO geometric features

5.1 Testing the effect of orifice arrangement (test 1)

This test aimed to determine the effects of different orifice arrangements on the pressure loss coefficient. Ten test plates with *EDR* (or *DR*)=0.4 were employed to perform this task, and their descriptions and photos are shown in Fig. 7. For the sake of brevity, the specific arrangement features of each MO are described in a simple manner as A1-B1-C1, where A1 represents *n*; B1 equals 1 or 0 to indicate whether or not the test plate has centered holes, respectively; and C1 is R or C indicating a rectangular or circular arrangement, respectively.

Fig. 8 shows each ξ value as a function of $\mathrm{Re_D}$. The results show that for lower $\mathrm{Re_D}$, ξ generally increases with $\mathrm{Re_D}$, while the difference between the test plates' ξ values appears to be much greater than that at higher $\mathrm{Re_D}$ values. When $\mathrm{Re_D}$ is near 10,000, there was a 47% deviation between the ξ value obtained from SO and that from 9-1-C. The difference gradually decreases to 17.7% when $\mathrm{Re_D}$ increases to 15,000, and then the difference remained stable for higher $\mathrm{Re_D}$ values. Meanwhile, $\mathrm{Re_D}$=15,000 represents a cut-off point at which the ξ values started to deviated from the regression lines, which are

represented as two continuous lines in Fig. 8.

Note that ξ is usually greater for test plates with fewer orifices. This behavior is displayed in Fig. 9, which shows the effect of orifice thickness evaluated in terms of s/d on the mean values of ξ. s/d represents the dimensionless orifice thickness, where s is the orifice thickness (detailed specifications were according to ISO5167-1) and was 2 mm for all test plates in this paper, and d is the restriction diameter of separated throttle holes.

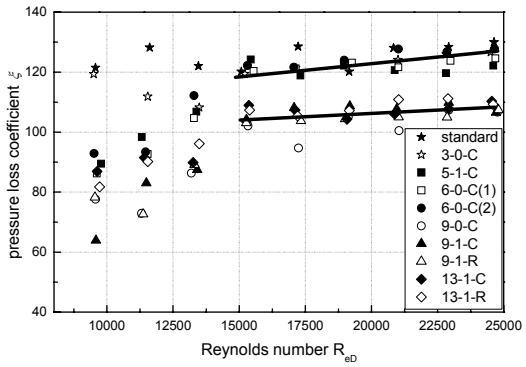

Fig. 8. Effect of the Reynolds number on the measured pressure loss coefficient (test 1).

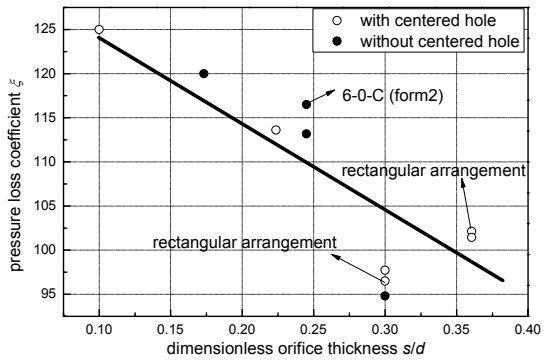

Fig. 9. Mean pressure loss coefficient vs. dimensionless orifice thickness (test 1).

According to Chisholm [7], all test plates here can be classified as thin plates due to their s/d values (s/d<0.5). ξ generally increases with decreasing s/d, with a 24% decrease in ξ observed when s/d is increased from 0.1 to 0.38. The minimum ξ was attained with an s/d ratio of 0.3, at which ξ undergoes a sharp decrease. This behavior can be ascribed to the pattern of orifice distribution, which induced a stronger decrease in ξ to overcome the influence of s/d. The data also reveal that various orifice arrangements result in different ξ values at the same s/d value, which is represented in Fig. 9 as three lines with arrowheads.

5.2 Testing the effect of geometric parameters (test 2)

In this test, test plates with fixed orifice arrangements such as 3-0-C, 6-0-C (form 2) and 9-0-C were used to investigate the influence of three geometric parameters on the pressure loss coefficient. Nine test plates were selected with various combinations of three different n values (n=3, 6, 9), three different EDR values (EDR=0.2, 0.3, 0.4) and three different D_d values (D_d=0.02, 0.04, 0.08). For the sake of brevity, the plates are referred to using the notation A2-B2-C2, where A2, B2 and C2 indicate the values of n, EDR and D_d, respectively. Fig. 10 shows images of and detailed information on these test plates.

Fig. 11 shows the overall test results in terms of ξ as a function of Re_D. As can be observed, the experimental data can be divided into three regions ranging from 1500 to 2000, 250 to 500 and 60 to 120. These regions are mainly characterized by different EDR values. For higher EDR values, the data have a lower dependence on Re_D. Meanwhile, the other two geometric parameters appear to have extremely weak effects on the pressure loss coefficient. These results demonstrate that EDR

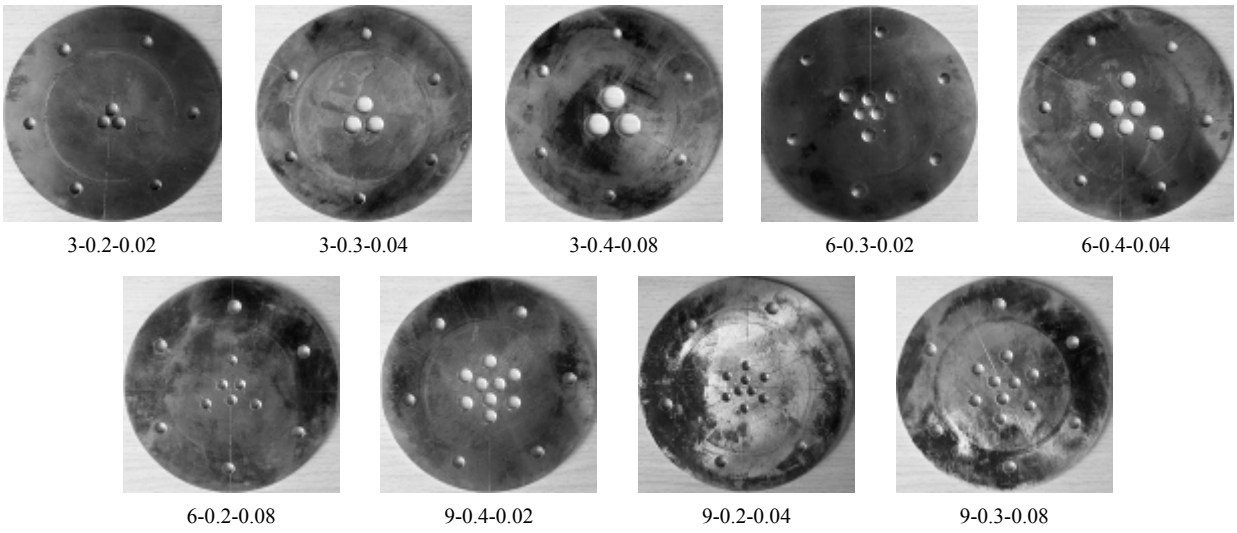

Fig. 10. Test plates employed in test 2.

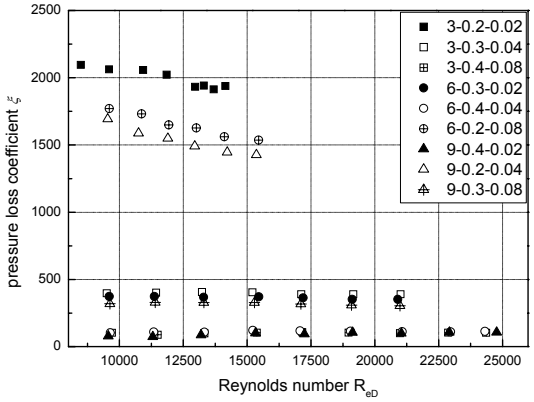

Fig. 11. Overall results of test 2.

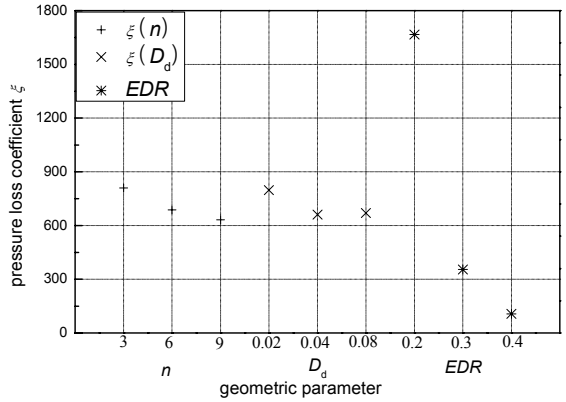

Fig. 12. Range values of the geometric parameters studied here.

has the dominant effect on pressure loss.

Fig. 12 presents more explicit evidence for the relationship between geometric parameters and the loss coefficient using the aid of range method. As can be observed, the range values for n, D_d and EDR were 177, 137 and 1560, respectively, demonstrating the overwhelming influence of EDR on ξ, especially for test plates with EDR values ranging from 0.2 to 0.3, due to the high range value in this domain (nearly 1400).

These data allowed us to conclude that EDR is the dominant geometric parameter because of its very strong influence on the ξ of MO, as seen in Fig. 10. Therefore, it is feasible to adopt EDR as the single parameter affecting ξ in a further modeling study.

6. Modeling the MO pressure loss coefficient

6.1 Testing the accuracy of the test rig using SOs according to ISO5167 (test 3)

Based on the investigations above, this test was designed to model the relationship between ξ and EDR using five 6-0-C test plates (form 2). First, we analyzed the detailed geometry of the MOs. As can be observed in Fig. 13,

$$D' < D \tag{9}$$

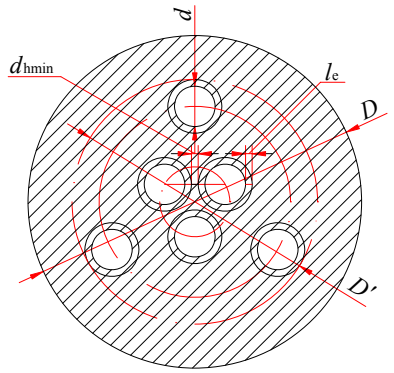

Fig. 13. Configuration schematic of 6-0-C (form 2).

$$D' = 4.155d + 8.31l_e + 3.154d_{h\,min} \tag{10}$$

$$EDR = \sqrt{6}\frac{d}{D} \tag{11}$$

$$D_d = \frac{d_{hmin}}{D}. \tag{12}$$

Starting from Eqs. (9)-(12), the relationship between EDR, D_d and l_e can be determined as

$$EDR < 0.59 - 1.86D_d - 4.9l_eD^{-1}. \tag{13}$$

Adopting a D_d value of 0.02, the EDR should be lower than 0.454 because of the test restrictions of D=50 mm and l_e=1 mm. According to the EDR range, ten test plates (shown in Fig. 14) including five 6-0-C (form 2) MOs with EDR=0.25, 0.3, 0.35, 0.4 and 0.45 (denoted as M-EDR) and five SOs (defined in ISO5167) with DR=0.25, 0.3, 0.35, 0.4 and 0.45 (denoted as S-DR) were chosen for this experiment. Because EDR and DR have the same geometric meanings for MO and SO, respectively, the results of this test can be compared to available correlations proposed in ISO5167 to investigate the reliability of the test data. The relevant equations can be generalized as:

$$\Delta P_{(D,D/2)} = 0.5\rho^{-1}\left(\frac{\mu}{D}\right)^2\left(\frac{\mathrm{Re_D}}{C}\right)^2(DR^{-4}-1) \tag{14}$$

where $\Delta P_{(D,D/2)}$ represents the pressure difference using the D and D/2 pressure tapping measurements.

The SO discharge coefficient C can be calculated using the Stolz equation (Eq. (15)) [11] and the Reader-Harris/Gallagher equation (Eq. (16)) [12] to determine the discharge coefficients according to ISO5167 (1991) [8] and ISO5167 (2003) [9, 10], respectively.

$$\begin{aligned} C &= 0.5959 + 0.0312DR^{2.1} \\ &-0.0184DR^8 + 0.0029DR^{2.5}(10^6/\mathrm{Re_D})^{0.75} \\ &+0.039L_1DR^4(1-DR^4)^{-1} - 0.0337L_2DR^3 \end{aligned} \tag{15}$$

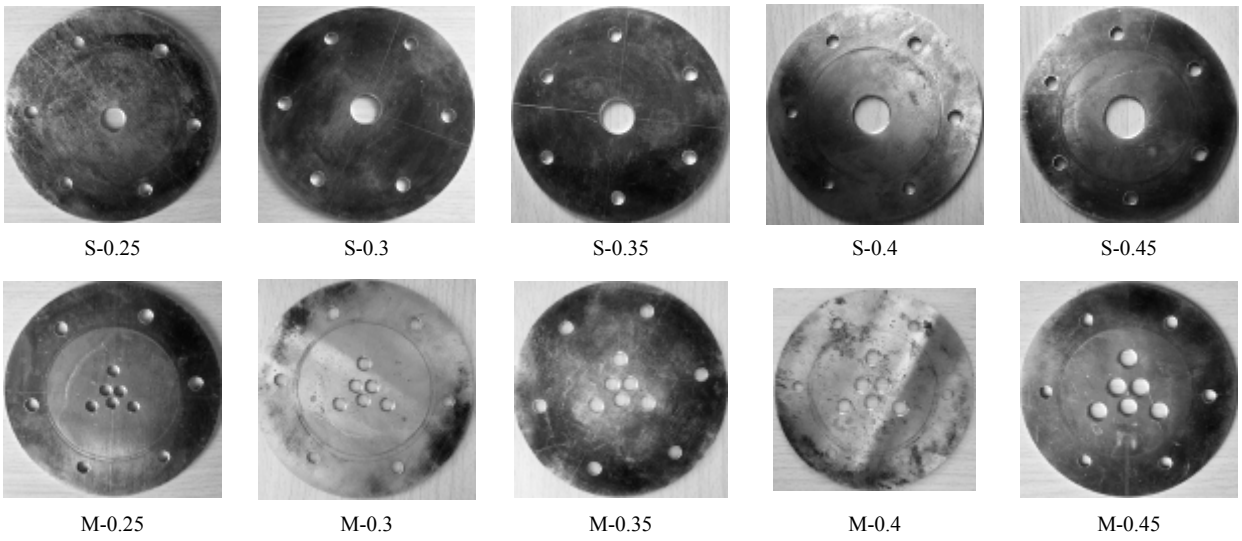

Fig. 14. Test plates employed in test 3 and test 4.

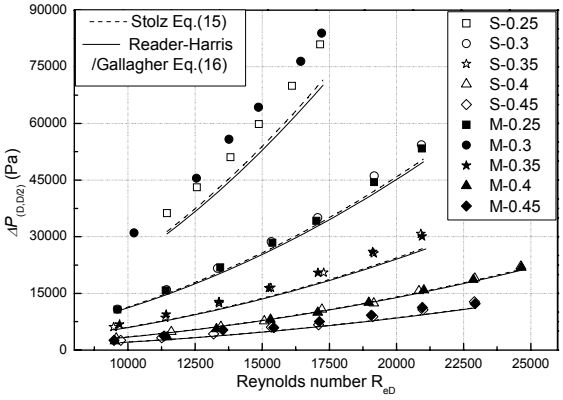

Fig. 15. Pressure difference between the D and D/2 pressure measurements as a function of the Reynolds number.

$$C = 0.5961 + 0.0261DR^2 - 0.216DR^8 + 0.000521(10^6\,DR/\mathrm{Re_D})^{0.7} + (0.0188 + 0.0063A)DR^{3.5}(10^6/\mathrm{Re_D})^{0.3} + (0.043 + 0.08e^{-10L_1} - 0.123e^{-7L_1})(1 - 0.11A)DR^4/(1 - DR^4) - 0.031(M - 0.8M^{1.1})DR^{1.3} + 0.011(0.75 - DR)(2.8 - D/25.4) \quad (16)$$

where L_1=1, L_2=0.47 for the D and D/2 pressure tapping measurements, and A=(19000DR/$\mathrm{Re_D}$)0.8, M=-2L_2/(1-DR).

Fig. 15 shows $\Delta P_{(D,D/2)}$ as a function of $\mathrm{Re_D}$. The experimental data were compared with the Stolz equation and the Reader-Harris/Gallagher equation.

As can be observed, near S-0.25, the experimental data are fit well by the correlations involving both the Stolz and Reader-Harris/Gallagher equations, especially for a higher DR(EDR) or a lower $\mathrm{Re_D}$. These comparisons may explain the reliability of this experimental set-up, and they indicate that the model is sufficiently accurate for use in a further modeling study on the ξ value of 6-0-C plates (form 2).

Furthermore, it is worth noting that the Stolz equation always over-estimates $\Delta P_{(D,D/2)}$ as calculated by the Reader-Harris/Gallagher equation, with 2%, 1.7%, 1.4%, 1.0% and 0.6% deviations for DR(EDR)=0.25, 0.3, 0.35, 0.4 and 0.45, respectively.

For the same $\mathrm{Re_D}$, the $\Delta P_{(D,D/2)}$ value of 6-0-C (form 2) was generally greater than that of SO, with a 6.5% deviation when DR (EDR)=0.25. The difference in $\Delta P_{(D,D/2)}$ decreases with increasing DR (EDR) values, with a 1.5% deviation as DR (EDR) =0.4. This trend also applies to $\mathrm{Re_D}$, as when DR (EDR) =0.3, the differences in $\Delta P_{(D,D/2)}$ were 0.9% and 3.8% at $\mathrm{Re_D}$=9600 and $\mathrm{Re_D}$=19,200, respectively.

6.2 Modeling the MO pressure loss coefficient (test 4)

For the MOs presented in Fig. 14:

$$\xi = Function(n, D_d, EDR)\,. \quad (17)$$

According to the results of test 2, Eq. (17) can be simplified as

$$\xi = Function(EDR)\,. \quad (18)$$

The model ξ=*Polynomial*(EDR)(EDR^C-1) was adopted for the ξ correlations. The results are shown in Fig. 16 with the following model description:

$$\xi(EDR) = P_m(EDR^{-4.448} - 1) \quad (19)$$

$$\xi(DR) = P_s(DR^{-4.187} - 1) \quad (20)$$

where

$$P_m = 160.325(71.467EDR^4 - 100.300EDR^3 + 52.021EDR^2 - 11.801EDR + 1),$$

$$P_s = 150.848(74.679DR^4 - 103.507DR^3 + 53.001DR^2 - 11.874DR + 1).$$

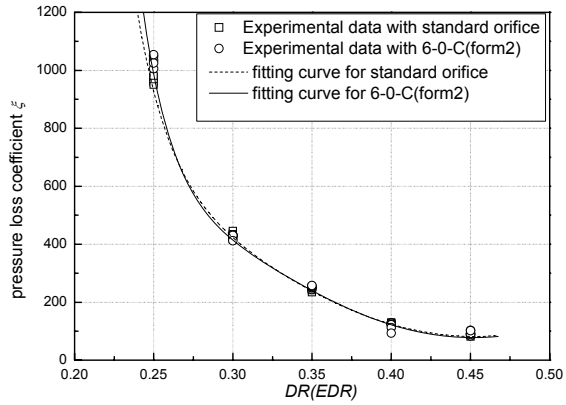

Fig. 16. Fitting curves vs. experimental data.

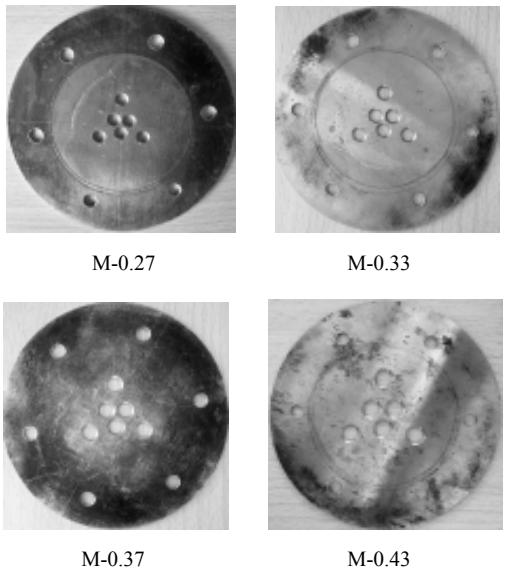

Fig. 17. Test plates employed in test 5.

As shown in Fig. 16, the two curves for SO and 6-0-C (form 2) exhibit almost the same trend when *DR* (*EDR*) is greater than 0.27. The ξ value of 6-0-C (form 2) was slightly greater than that of an SO when the *DR* (*EDR*) was lower than 0.27.

6.3 Validation of the ξ model (test 5)

To verify Eq. (19), another four 6-0-C (form 2) plates with *EDR*= 0.27, 0.33, 0.37 and 0.43 were tested, as shown in Fig. 17. The results are presented in Fig. 18. Note that Eq. (19) agrees well with the experimental data obtained from the four test plates when *EDR* ranged from 0.25 to 0.45.

7. Conclusion

This paper introduced an MO structural design methodology and implemented it experimentally. First, the MO structure was quantified through the geometric architecture. Then, experiments were used to simplify and further develop the correlation between MO geometric features and ξ. The final ξ model is highly accurate, indicating that the methodology used here is effective.

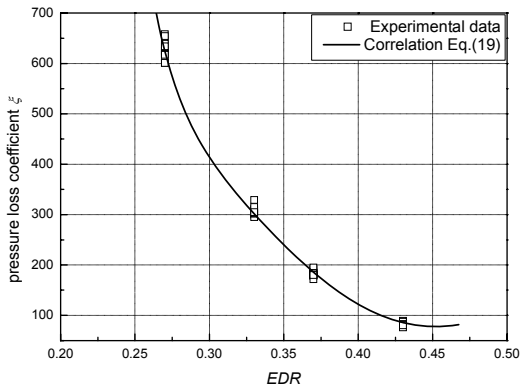

Fig. 18. Model validation results.

This study leads to the following conclusions:

(1) The ξ values of MOs are generally higher for MOs with fewer perforated holes. Even though all test plates can be classified as thin orifices, the *s*/*d* value is the dominant factor determining the MO ξ value, and the orifice arrangement is also an important aspect affecting the MO ξ value.

(2) The orifice arrangement of MOs can be expressed by three key parameters: the total orifice number, *n*; the equivalent diameter ratio, *EDR*; and the distribution density, D_d. *EDR* has a dominant influence on the MO ξ value compared with the other two parameters.

(3) The geometric factors can be ranked according to decreasing effect on ξ as *EDR*, *n*, D_d, *s*/*d* and orifice arrangement form.

(4) The relationships between *EDR* and *DR* were used to compare available correlations with the test data. This comparison revealed that the test apparatuses had an acceptable accuracy, as the results fit with correlations using either the Stolz or Reader-Harris/Gallagher discharge coefficient models.

(5) The model obtained in the present paper provides a reliable MO ξ prediction with *EDR* values ranging from 0.25 to 0.45. The test procedures may also be applied to MOs with other orifice arrangements.

(6) The design methodology and test procedure presented in this work allow for the simplification of the structural design of MOs. This work also provides a good reference for further studies of MO throttle characteristics in two-phase flow systems.

Acknowledgment

The research presented in this paper was financially supported by the National Natural Science Foundation of China (Grant No. 51008042, No. 51078053), the Fundamental Research Funds for the Central Universities of China (No. DUT11ZD105) and by China Postdoctoral Science Foundation (No. 20100481235).

Nomenclature

AE : (Effective) work potential absolute error value
C : Exergy discharge coefficient
D : Energy of a system inner diameter of pipe, m
D' : External edge diameter, m
D_c : Diameter of center circle, m
D_d : Orifice distribution density
DR : Diameter ratio of single-hole orifice
d : Orifice restriction diameter, m
d_{hmin} : Minimum spacing between the edges of orifices located at adjacent center circles, m
EDR : Equivalent diameter ratio of multi-hole orifice l_e difference between the orifice edge radius and the orifice radius, m
n : Total number of orifices
P_v : Velocity pressure, Pa
$\Delta P_{(D,D/2)}$: Pressure difference using D and D/2 tapping measurements, Pa
ΔP_f : Pressure difference across orifice determined using a flowmeter, Pa
ΔP_s : Static pressure difference across the test plate, Pa
p_{sd} : Static pressure downstream, Pa
p_{su} : Static pressure upstream, Pa
Q_v : Volume flow, m^3/s
RE : Relative error value
s : Orifice thickness, m
v : Mean velocity, m/s
ξ : Pressure loss coefficient
μ : Dynamic viscosity, Pa•s
ρ : Water density, kg/m^3

References

[1] A. B. C. Anderson, A circular-orifice number describing dependency of primary frequency on differential pressure, gas density and orifice geometry, *Journal of Acoustical Society of America*, 25 (1953) 626-631.
[2] P. Testud, P. Moussou, A. Hirschberg and Y. Auregan, Noise generated by cavitating single-hole and multi-hole orifices in a water pipe, *Journal of Fluids and Structures*, 23 (2) (2007) 163-189.
[3] G. H. Gan and S. B. Riffat, Pressure loss characteristics of orifice and perforated plates, *Experimental Thermal and Fluid Science*, 14 (2) (1997) 160-165.
[4] G. Kojasoy, P. Kwame-Mensah and C. T Chang, Two-phase pressure drop in multiple thick and thin orifices plates, Experimental Thermal and Fluid Science, 15 (4) (1997) 347-358.
[5] M. Fossa and G. Guglielmini, Pressure drop and void fraction profiles during horizontal flow through thin and thick orifices, Experimental Thermal and Fluid Science, 26 (5) (2002) 513-523.
[6] A. A. Saadawi, E. Grattan and W. M. Dempster, Two-phase loss in orifice plates and gate valves in large diameter pipes, in: G. P. Celata, P. Di Marco, R. K. Shah (Eds.), 2nd Symp. Two-Phase Flow Modeling and Experimentation. ETS, Pisa, Italy (1999).
[7] D. Chisholm, Two-phase flow in pipelines and heat exchangers, Longman Group Ed, London (1983).
[8] International Organization for Standardization, Measurement of fluid flow by means of pressure differential devices—part 1: orifice plates, nozzles and Venturi tubes inserted in circular cross-section conduits running full, ISO 5167-1. International Organization for Standardization, Geneva (1991).
[9] International Organization for Standardization, Measurement of fluid flow by means of pressure differential devices—part 1: orifice plates, nozzles and Venturi tubes inserted in circular cross-section conduits running full, ISO 5167-1. International Organization for Standardization, Geneva (2003).
[10] International Organization for Standardization, Measurement of fluid flow by means of pressure differential devices—part 2: orifice plates. International Organization for Standardization, Geneva (2003).
[11] J. Stolz, A universal equation for the calculation of discharge coefficients of orifice plates, In Flow Measurement of Fluids (ed. H.H.Dijstelbergen and E.A.Spencer), North Holland, Amsterdam (1978) 519-534.
[12] M. J. Reader-Harris, J. A. Sattary and E. P. Spearman, The orifice plate discharge coefficient equation-further work. Flow Meas. Instrum., 6 (2) (1995) 101-144.

Zhao Tianyi is a postdoctoral researcher in HVAC department at Dalian University of Technology, Dalian, China, 2009. He received his Ph.D degree in School of Municipal & Environmental Engineering, Harbin Institute of Technology, Harbin, China, 2005-2009. His research interests are optimal control of HVAC equipment and system, and design and development of novel HVAC equipment.